



## SOURCE, BASIN, AND SITE EFFECTS IN STRONG MOTION RECORDS OF THE 2015 GORKHA EARTHQUAKE

D. Asimaki<sup>(1)</sup>, E. M. Thompson<sup>(2)</sup>, S. Rajaure<sup>(3)</sup>, S. E. Hough<sup>(4)</sup>, P. Ampuero<sup>(1)</sup>, S. Martin<sup>(5)</sup>

<sup>(1)</sup> Professor, California Institute of Technology, Pasadena, California, USA, [domniki@caltech.edu](mailto:domniki@caltech.edu)

<sup>(2)</sup> Research Geophysicist, U.S. Geological Survey, Golden, Colorado, USA, [emthompson@usgs.gov](mailto:emthompson@usgs.gov)

<sup>(3)</sup> Senior Divisional Geologist, Department of Mines and Geology, Lainchaur, Kathmandu, Nepal, [srajaure@gmail.com](mailto:srajaure@gmail.com)

<sup>(4)</sup> Senior Seismologist, U.S. Geological Survey, Pasadena, California, USA, [hough@usgs.gov](mailto:hough@usgs.gov)

<sup>(5)</sup> Research Assistant, Earth Observatory of Singapore, Nanyang Technological University, Singapore, [smartin@ntu.edu.sg](mailto:smartin@ntu.edu.sg)

### ***Abstract***

The M7.8 Gorkha, Nepal mainshock ruptured a segment of the Main Himalayan Thrust directly below Kathmandu Valley, causing strong shaking levels and extensive structural damage across the valley. Strong motion data reveal an initial 6-s source pulse followed by 4-6 s energy reverberating within the basin. One of the striking features of the observed ground motions in the valley is that they were depleted of energy in the 0.5-10 Hz frequency range, which likely limited the severity of the structural damage compared to other possible realizations of similar ruptures. Isolated cases of liquefaction and lateral spreading of unconsolidated sediments were also observed but have not yet revealed a systematic damage pattern. Initial analysis of available data suggests that several different factors, including source and path as well as site effects, were responsible for the unusual character of the ground motions. In this paper, we review earthquake reconnaissance as well as available strong motion records from Kathmandu Valley to better understand the observations from this earthquake.

*Keywords: Site effects; Basin response; Damage distribution*

## 1. Introduction

The 2015 Gorkha earthquake ruptured the segment of the Main Himalayan Thrust direct beneath the Kathmandu Valley. The large magnitude and proximity to the valley caused strong shaking in Kathmandu, and caused significant structural damage (Fig. 1a) and thousands of landslides [1] (Fig 1b). The few instrumental records of ground shaking that are now available indicate that the ground motions were relatively depleted in high-frequency energy compared to what would be expected on average for earthquakes of similar size and distance [2]. Hayes et al. [3] summarized the rapid characterization of the event by the U.S. Geological Survey; notwithstanding the lack of instrumental recordings that were available at the time and the peculiar nature of the ground motion frequency content, within 4 hours after the mainshock, the U.S. Geological Survey estimated that this event resulted in around 9,000 fatalities and Modified Mercalli Intensity (MMI) up to IX. This fatality estimate is consistent with the best currently available estimates, and a subsequent detailed study of structural damage [4] concluded that European Macroseismic Scale (EMS) intensities peaked in the VII-VIII range, which is slightly less than expected. Currently, we have access to five strong motion records of the mainshock. These records show that this event was characterized by a long period (5 sec) predominant pulse that reverberated in the valley for 4-5 cycles before gradually decaying, and a surprisingly low peak ground acceleration (PGA) of 0.16g. High rate (5 Hz) GPS measurements recorded within the basin and on the surrounding mountain ranges (source: UNAVCO) are consistent with the strong motion records at frequencies below 0.5 Hz, which includes the 5 sec pulse.

The Kathmandu Valley has experienced numerous large earthquakes in the last 1500 years [5, 6]. The most recent large event was the M8.1-8.4 Great Nepal-Bihar Earthquake of 1934 [7–11]. This event caused about 8,500 casualties and destroyed 20 percent and damaged 40 percent of the valley's building stock, including one quarter of the buildings in Kathmandu and many of the temples in Bhaktapur [6]. Within the basin, estimated intensities correlated qualitatively to the depth of the basin sediments, suggesting that site effects played a major role in modifying the 1934 event's ground motion within Kathmandu [12]. A number of studies have concluded that the 1934 earthquake damage was accentuated by ground motion amplification in the fluvio-lacustrine sediments of the southern Kathmandu Valley and by liquefaction [6, 8, 13–15].

While the importance of site response in the valley has long been clear, strong motion data have been scarce and sparse, and the detailed nature of site effects has thus remained poorly understood. To date, site response studies in the Kathmandu Valley have relied almost exclusively on microtremor data (e.g., [14, 16, 17]). Strong motion recordings from the 2015 Gorkha earthquake sequence provide a unique opportunity to better understand site effects on multiple spatial and frequency scales: we specifically analyze ground motions from the 25 April 2015 Gorkha mainshock (M 7.8), and compare them to the 12 May Dolakha aftershock (M 7.3) and other moderate-to-large aftershocks recorded at five strong motion stations (four of which are located on unconsolidated sediments and one on reference rock) and two high-rate GPS records. Our analysis reveals that a combination of nonlinear site response and source characteristics can explain the mainshock anomalously long period character of the ground motion shaking.

## 2. Geology of the Kathmandu Basin

The Kathmandu Basin lies on the Kathmandu Nappe [18] along the southern slopes of the Himalaya. A lake occupied a large part of the basin from Pliocene to Pleistocene [19]. The basin is currently filled with a very thick (500–600 m) sequence of fluvio-lacustrine sediments [20] and is bounded to the south by a tectonic ridge developed above the Main Boundary Thrust (MBT). On the northern part of the valley, sediments are poorly sorted, thin- to medium-bedded highly micaceous coarse sands, gravel, and silts interlayered with clays. In the south, they consist of a thick sequence of dark grey to black highly plastic clay and silts, usually overlain and underlain by coarse sediments. The black plastic clay (locally called Kalimati or *black cotton*) is rich in organic matter. The age of this clay is placed in the Pliocene to Pleistocene time according to Yoshida and Igarashi [19]. The maximum thickness of the Black Clay is approximately 300 m, and is greatest along the central part of the valley starting from Satungal towards Lalitpur and Bhaktapur (Fig. 2(a)).



Fig. 1 – (a) Complete collapse of ground floor of a multistory reinforced concrete frame with infill masonry wall construction on slopes due to soft story effect coupled with ground failure (photo by Kishor Jaiswal at the U.S. Geological Survey); and (b) Rock slide along the Kali Gandaki River (reproduced from [1]).

The sedimentation processes in the Kathmandu Valley are controlled by the regional fault activity, and the drainage system of the surrounding mountains. According to Sakai et al. [22], the active faults related to the basin sediment formation are in the southern part of the valley, the Chandragiri Fault and the Chobhar Fault, which run through the colluvial slopes and terraces of the late Pleistocene; and in the northwestern part of the valley, the Kalphu Khola Fault, which runs through the late Pleistocene gneissic boulder beds [23]. The complex tectonic environment surrounding the Kathmandu basin is shown in Fig. 2(b). As a consequence of this environment, the geology of the valley is strongly heterogeneous: the southern sediments are predominantly composed of weathered meta-sedimentary rocks from the southern hills such as Chandragiri and Phulchauki, and the northern sediments are composed of weathered gneiss and granites from the northern Shivapuri Hills.

### 3. Strong motion records

Following the 2011 Himalayan earthquake in the Kathmandu Valley, the Central Department of Geology (CDG) at Tribhuvan University (TU) installed four Mitsutoyo JEP-6A3-2 accelerometers in collaboration with Hokkaido University, Japan [24]. The strong motion stations have a 100 Hz sampling rate and are operated on continuous recording mode. One of the strong motion stations, KTP, was installed on rock outcrop at the Kirtipur Municipality Office, and the other three accelerometers (TVU, PTN, THM) were installed on sediments, along an east-west linear array across the valley. In addition to the above instruments, the U.S. Geological Survey (USGS) installed one (GeoSIG NetQuakes) 200 Hz accelerometer on sediments [25]. The Department of Mines and Geology also operated a strong motion instrument in central Kathmandu, which also recorded the 2015 sequence [26]. The code names and locations of all stations are shown in Fig. 3b. In this paper, we analyze ground motions at these stations from the 25 April 2015 M7.8 Gorkha earthquake, the 12 May 2015 M7.3 Dolakha earthquake, and two smaller aftershocks: the 26 April 2015 M6.7 and the 25/04/2015 M6.6 events (Fig. 3a).

The epicenters of the M7.8 Gorkha mainshock and M6.6 25/4/2015 aftershock were located approximately 80 km NW of the Kathmandu Valley, while the epicenters of the M7.3 and 26/4/2015 M6.7 aftershocks were located approximately 80 km northeast of the valley. These events were also recorded by the two high-rate GPS stations shown in Fig. 3, namely KKN4 (installed on rock outcrop) and NAST (installed on the valley sedi-

ments). The mainshock and Dolakha aftershocks occurred on the Main Himalayan Thrust (MHT) [27], with mechanisms that are consistent with previously published fault plane solutions [28–30].

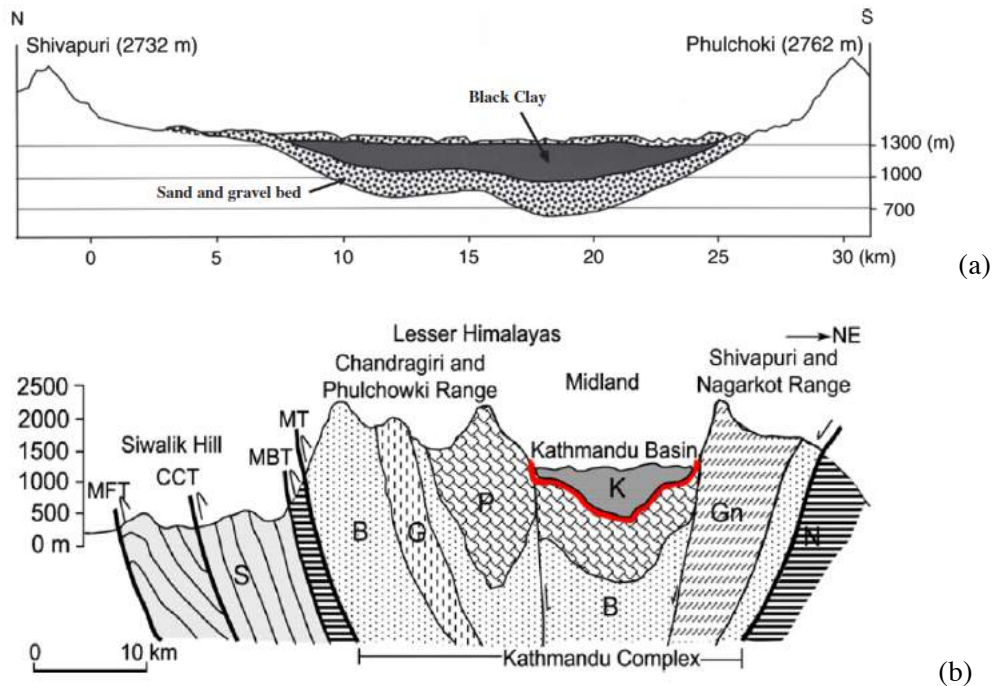


Fig. 2 - (a) Schematic of the Kathmandu Valley sediment deposits, reflecting the sedimentation processes; and (b) A schematic geologic cross-section through central Nepal (after Sakai et al. [23] and Stöcklin [31] and Bhattarai [26]). Capital letters correspond to the nomenclature developed by Sakai et al. to describe the Kathmandu basin geology: Siwalik Group, B: Bhimphedi Group, P: Phulchauki Group, N: Nawakot Complex, G: Granite, Gn: Gneiss Complex, K: Kathmandu Complex, MFT: Main Frontal Thrust, CCT: Central Churia Thrust, MBT: Main Boundary Thrust, MT: Mahabharat Thrust. Further details can be found in Mugnier et al. [32].

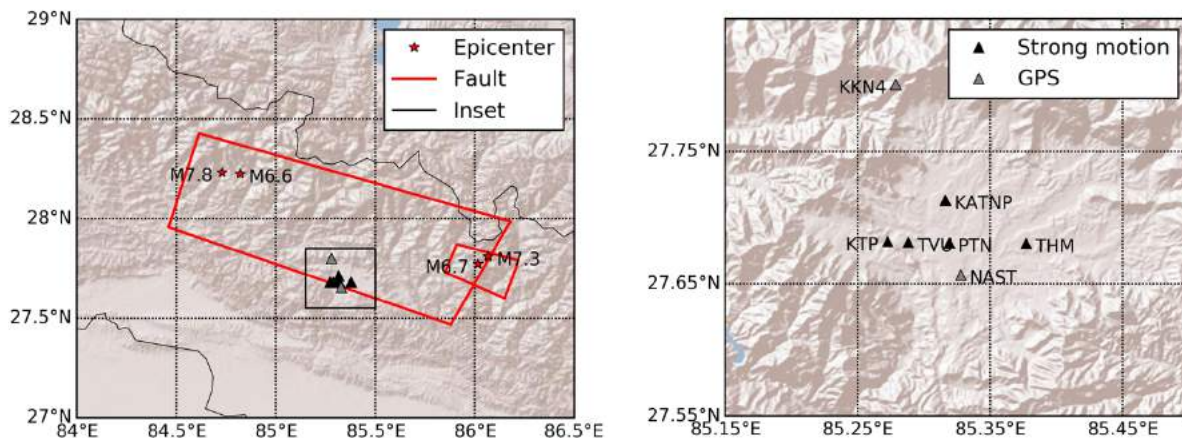


Fig. 3 – (left) Map depicting the epicenters of the 04/25/2015 M7.8 Gorkha and M6.6 25/4/2015 west of the valley and the 05/12/2015 M7.3 Dolakha and 26/4/2015 M6.7 earthquakes on the east. Approximate surface projections of the M7.8 and M7.3 events are also given from the USGS ShakeMap event pages (<http://earthquake.usgs.gov/earthquakes/eventpage/us20002926>, <http://earthquake.usgs.gov/earthquakes/eventpage/us20002ejl>). (right) inset showing the Kathmandu Valley and the locations of the five strong motion stations and two GPS stations used in this study.

Acceleration time series and peak ground accelerations for all strong motion stations and the two strongest events are indicated on Fig. 4. The rock-outcrop (reference) station of the array, KTP, recorded the maximum horizontal ground acceleration during the M7.8 mainshock ( $2.54 \text{ m/s}^2$  in the EW-direction); while the easternmost station of the array, THM, recorded the maximum horizontal acceleration during the M7.3 aftershock ( $1.66 \text{ m/s}^2$  in the EW direction). The response spectra of the mainshock and thereafter shown in Fig. 5. Moving from west to east, parallel to the M7.8 rupture below the valley, the low period (high frequency) energy depicted as a spike at 0.3 sec at station KTP gradually decays as the long period 5 sec pulse emerges, most clearly at stations KATNP and THM.

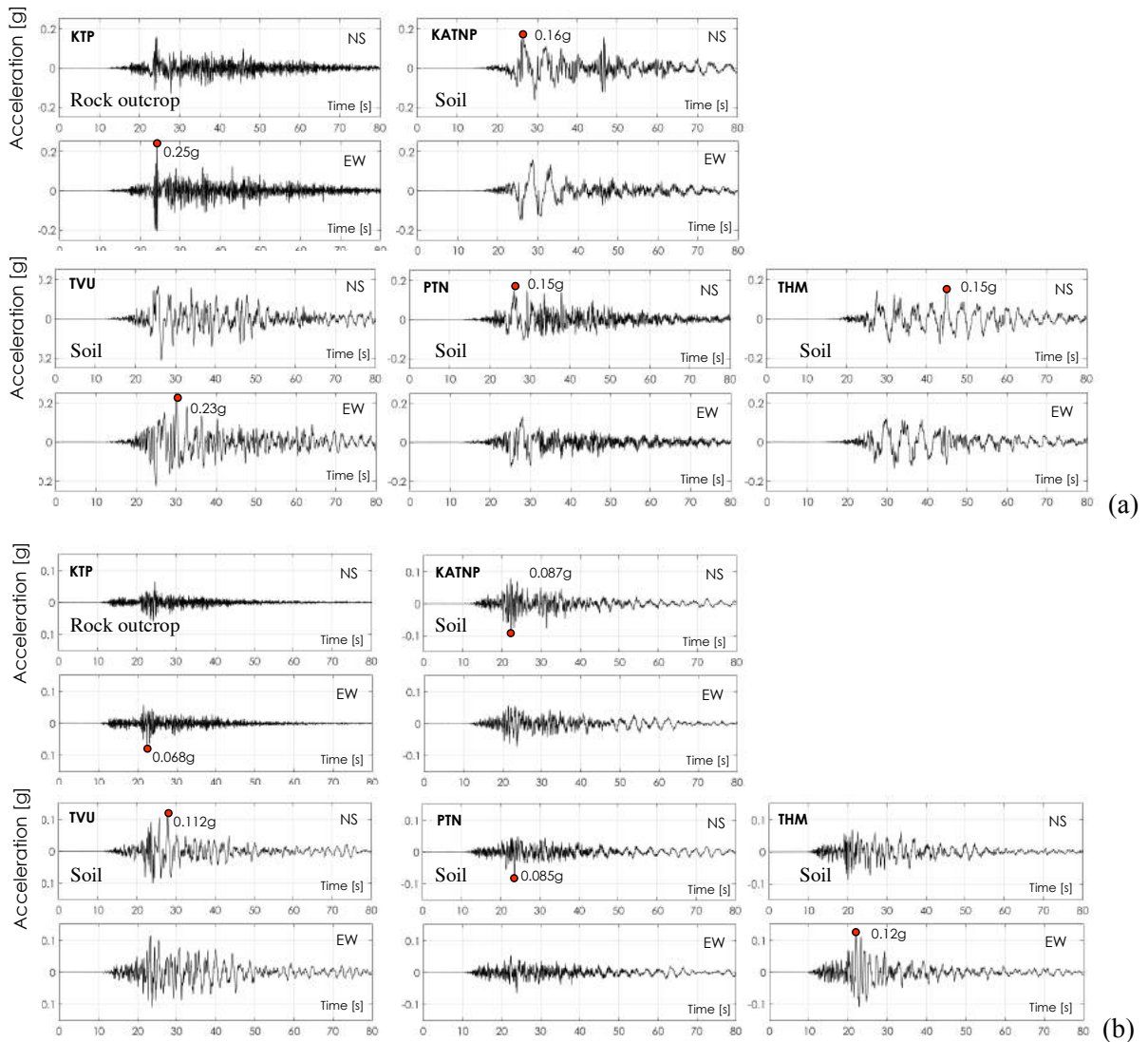


Fig. 4 - NS and EW components of the 04/25/2015 M7.8 Gorkha and the 05/12/2015 M7.3 Dolakha earthquakes recorded at the five strong motion stations.

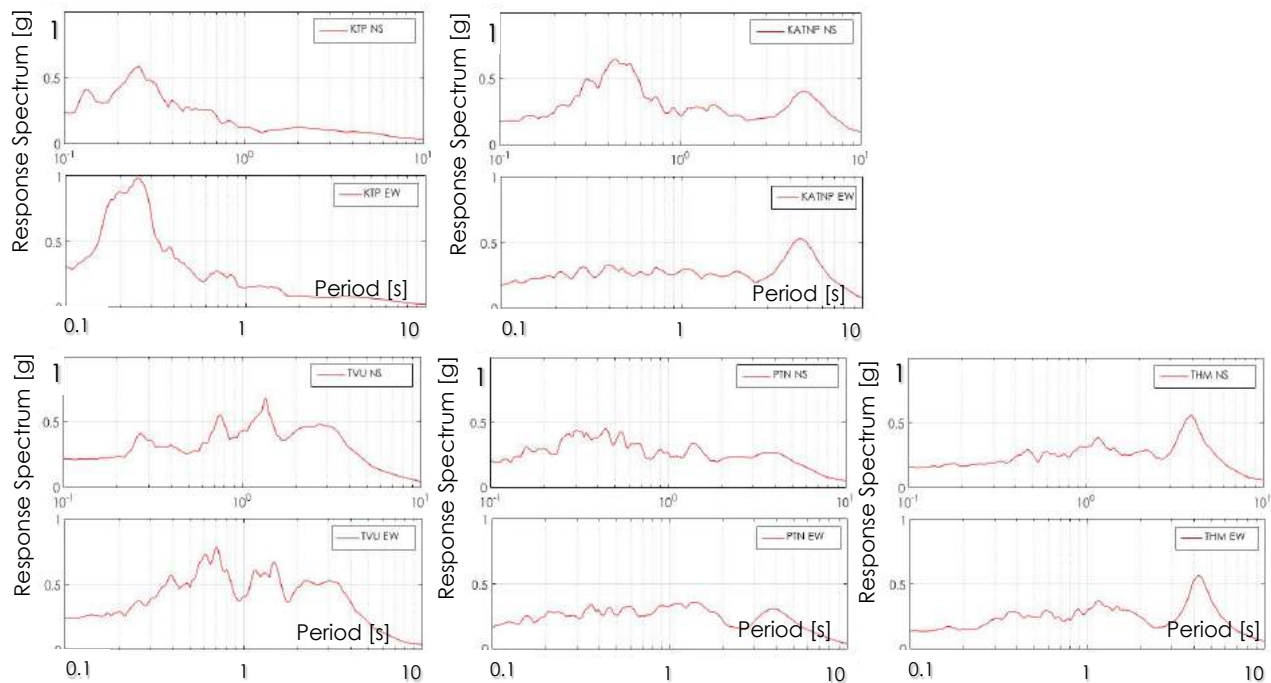


Fig. 5 - Response spectra of the NS and EW components of the 04/25/2015 M7.8 Gorkha mainshock.

#### 4. Site effects

We next use the strong motion records of the mainshock and three aftershocks to investigate site response relative to the reference rock site. The most striking characteristics of the ground motions at the four soil sites (TVU, PTN, THM, KATNP) are the large amplitude surface waves that dominate the time-series, and their severely attenuated high-frequency content. Fig. 6 shows the Fourier amplitude spectral ratios of the horizontal components (vector summation of NS and EW components) of the soil stations relative to the rock station (KTP). Fig. 6 shows the systematic strong amplification of all ground motions on soil compared to that on rock outcrop over a wide range of frequencies (approximately 0.1Hz - 2Hz), and deamplification of the frequency components larger than approximately 2 Hz. In the same figure, we also observe that the site response is characterized by three or more prominent peaks at approximately the same frequency range across all stations, which strongly suggests that all four soil stations (and by extension the basin sediments) are dominated by three common amplification mechanisms. In addition, we observe that systematically, site response during the M7.8 and M7.3 events is shifted to lower frequencies and has lower amplitude than the response to the M6.6 and M6.7 events correspondingly, results that suggest that the site response during the stronger events was nonlinear [15, 25].

We next consider the rotation independent response spectral acceleration RotD50 [33] of the M7.8 mainshock and M7.3, M6.7 and M6.6 aftershocks against response spectra predicted using a series of ground motion prediction equation (GMPEs). For this comparison, we have assumed time-averaged shear wave velocity of the top 30 m  $V_{S30}=200$  m/s for the soil sites [34]. Selecting a GMPE to compare our recordings against has proven to be challenging; given the seismotectonic environment in Nepal, a subduction zone GMPE would have been best. However, among the available choices, Atkinson and Boore [35] is outdated and has been severely downweighted in the U.S. National Seismic Hazard Maps [42]; the Zhao et al. model [36] was developed for Japan and doesn't have any data in the magnitude-distance range of interest (in this case,  $R_{jb} = 0$  km); the Atkinson and Macias model [37] is based on stochastic simulations tailored to the Cascadia subduction zone; the Ghofrani and Atkinson model [38] was recently developed on the basis of the M9.0 2011 Tohoku data and simulations. Among the available subduction zone options, the 2015 update to BC Hydro [39] was initially appealing since it is 'global,' has reasonable data coverage for the magnitude-distance range of interest, and

contrary to the above options, accounts for nonlinear response; however, it still doesn't have any data from the Himalayas, and it is impossible to evaluate its suitability on the basis of one earthquake sequence. And while the closest option geographically is the Sharma et al. model [40], validating our implementation of their equations was unsuccessful. Comparison between some of these alternative GMPEs is given in in Fig. 7, which clearly shows—if nothing else—wide variability in the predictions and no single GMPE performing especially well across all events, stations, and periods.

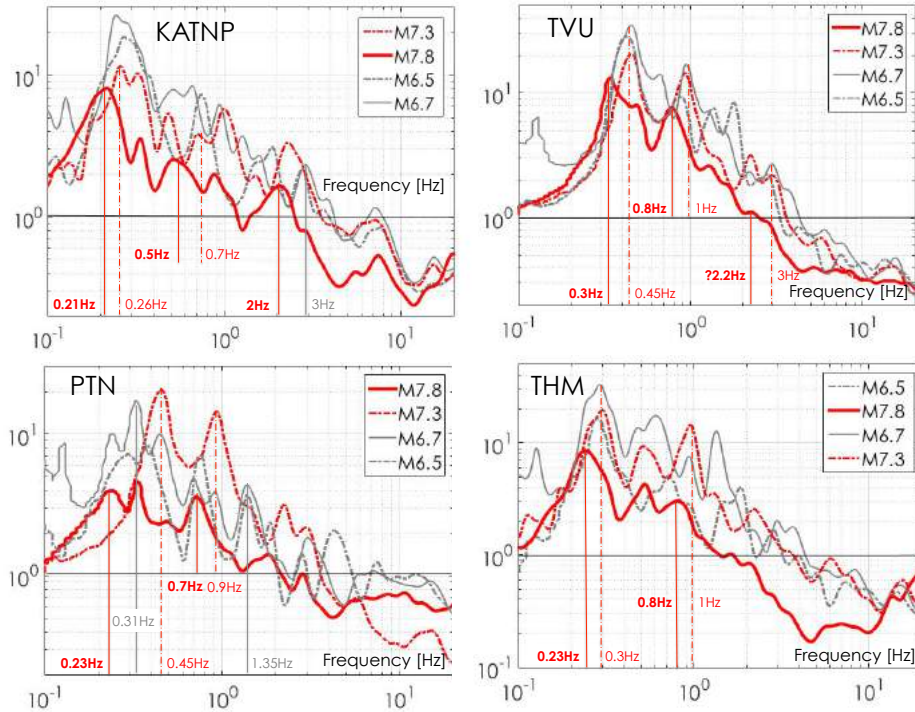


Fig. 6 – Soil amplification (transfer function) at the stations on soil relative to KTP. The systematic shift of the site response peaks to lower frequencies during the stronger events, as well as the reduction in amplitude are clear manifestations of nonlinear response. At each site, nonlinearity is observed at several frequencies (red vertical lines). We hypothesize that the ubiquitous lower frequency peak at 0.25 Hz represents amplification due to basin edge generated surface waves; while the middle and highest frequency peaks represent each amplification of the deeper and shallow soft soil layers correspondingly.

Although the Boore et al. [41] equations (BSSA14) were developed primarily on the basis of ground motions from the western United States (WUS), they provide a reasonable analog for Nepal as both are active crustal regions. Comparison of all four events to the BSSA GMPEs at all stations reveals that ground motions on soil are severely depleted of high-frequency (short-period) energy relative to predicted levels for M7.8 (Fig. 8). Note that while this high-frequency anomaly of the mainshock is more pronounced in the records on sediments, it is also present at the reference site KTP (Fig. 8), suggesting that the depletion of high-frequency effects is at least in part due to source and/or path effects rather than site effects alone. In the following sections, we explore the extent to which ground motions might have been controlled by both path and site effects.

## 5. Source and path effects

As we showed above, the mainshock strong motion records at all stations, including the reference rock site (KTP), were severely depleted of high-frequency energy relative to predicted levels for a M7.8 event below Kathmandu. This suggests that the depletion of high-frequency effects resulted from a combination of source and/or path and site effects.

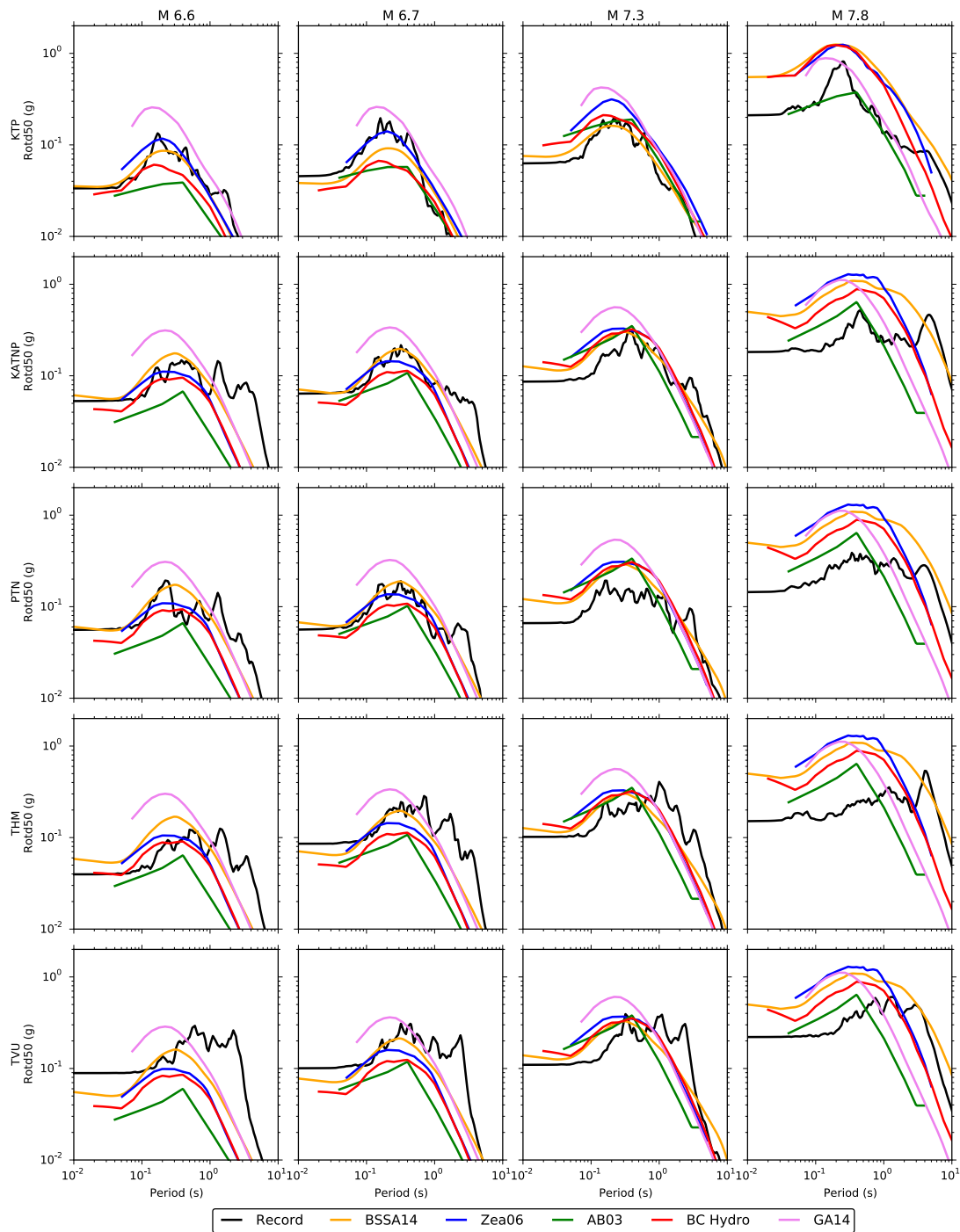


Fig. 7 - Orientation independent response spectral acceleration (RodD50) of the M7.8 Gorkha earthquake recorded at the five strong motion stations compared to the four subduction GMPEs and BSSA14. We assume the time-averaged shear-wave velocity in the upper 30 m ( $V_{S30}$ ) is 750m/s for the rock (reference) site, and 200 m/s for the soil sites, based on a small number of shear-wave velocity profiles published [34].

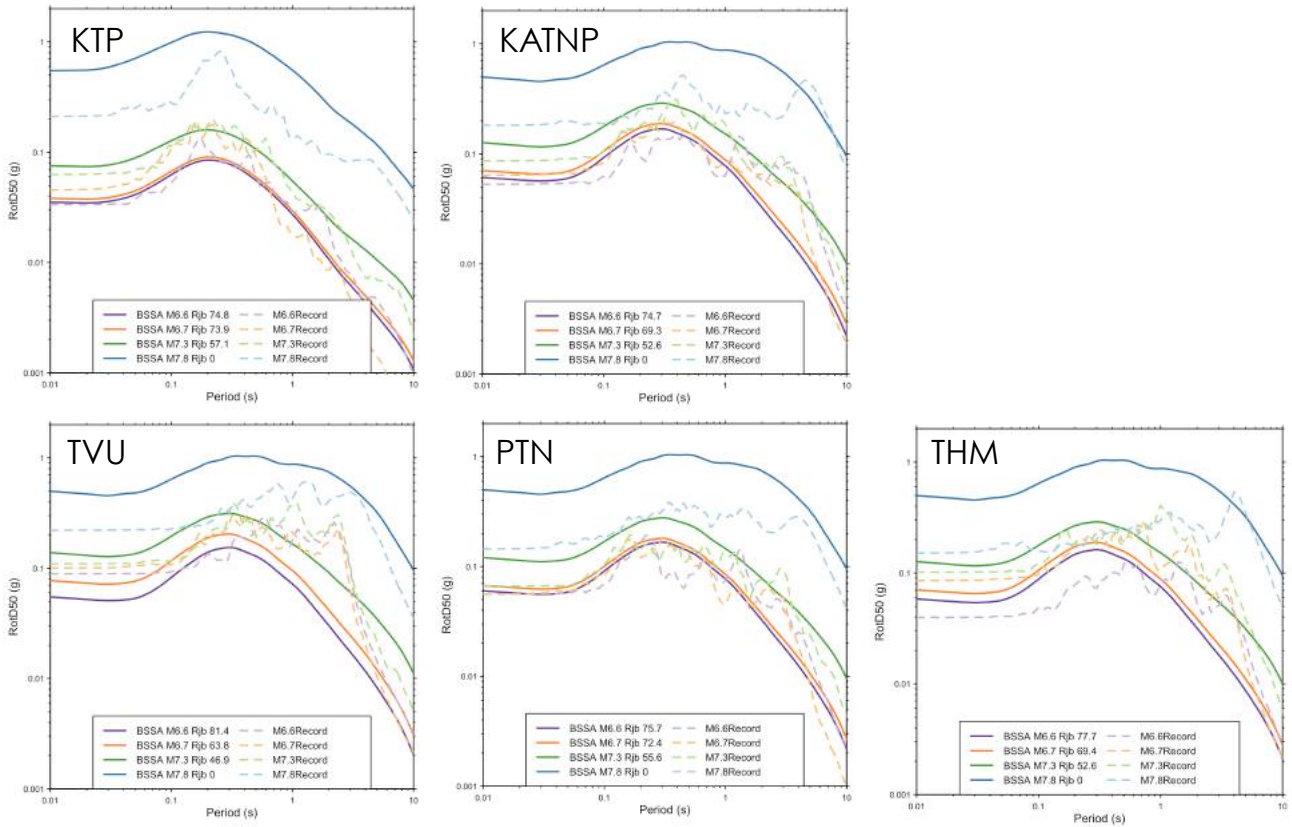


Fig. 8 - Orientation independent response spectral acceleration (RodD50) of the M7.8 Gorkha earthquake and the M7.3, M6.7 and M6.6 aftershocks recorded at the five strong motion stations compared to the BSSA14 GMPE [41]. We assume the time-averaged shear-wave velocity in the upper 30 m ( $V_{S30}$ ) is 750m/s for the rock (reference) site, and 200 m/s for the soil sites, based on a small number of shear-wave velocity profiles published [34].

According to Rajaure et al. [15] and Ampuero (written communication), this effect could be explained because the high-frequency energy in this earthquake was not uniformly distributed across the ruptured area. Although it is likely that the high-frequency energy is not uniformly distributed in any earthquake, particularly location of the strong motion stations relative to the fault has induced a bias in the distance to the high-frequency energy. The high-frequency energy was imaged by Avouac et al. [27]. Fig. 9 shows that the high-frequency energy was generally farther from Kathmandu Valley than the fault. GMPEs such as Boore et al. [41] are generally based on the nearest distance to the rupture, and this simple parameterization of distance cannot account for details such as the location of the high-frequency energy. For illustration purposes, we define  $R_{hf}$  as the nearest distance to concentrated region of high-frequency energy release. Given the nearly flat geometry of the mainshock rupture,  $R_{hf}$  is therefore significantly larger than the Joyner-Boore distance ( $R_{jb}$ ). For the stations we consider in this paper,  $R_{hf}$  is approximately 35 km, while  $R_{jb}$  is approximately 0 km. To fully consider the extent to which this difference can explain the depletion of high-frequency energy in Kathmandu would require comparison to GMPEs developed using  $R_{hf}$  rather than  $R_{jb}$ . Such relationships, however, are unavailable. For illustration, therefore, we consider how the Gorkha mainshock ground motions compare with Boore et al. [41] predictions assuming a distance of 35 km rather than 0 km (Fig. 10). It is interesting to note that the observed high-frequency (short-period) amplitudes more closely match the GMPE for  $R_{jb} = 35$  km, which is representative of the distance to the high-frequency energy as imaged by Avouac et al. [27], while the observed low-frequency (long-period) amplitudes more closely match the GMPE for  $R_{jb} = 0$  km.

## 6. Conclusions

In this paper, we have analyzed the mainshock and three aftershocks of the Gorkha earthquake sequence, as recorded on five strong motion records. These records reveal a mixture of features that have been frequently observed in similar settings, such as nonlinear response and strong amplification of long-period energy within the sedimentary basin. On the other hand, the lack of high-frequency energy in the mainshock was not something that was anticipated. Since this feature was not observed in the aftershock records, we expect that this is a feature that originated as a source characteristic, which can be explained by the confinement of the high-frequency energy at the deeper portion of the fault, which is on the distant side of the fault relative to Kathmandu Valley.

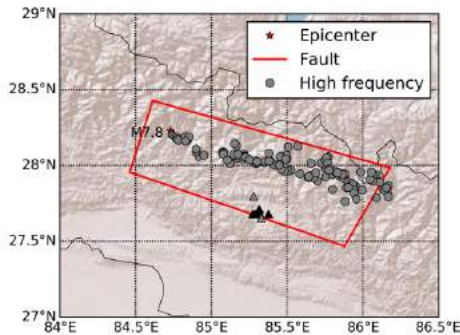


Fig. 9 – Back-projection of high-frequency radiation [27] depicting the concentration of these sources at a 35 km distance from the valley.

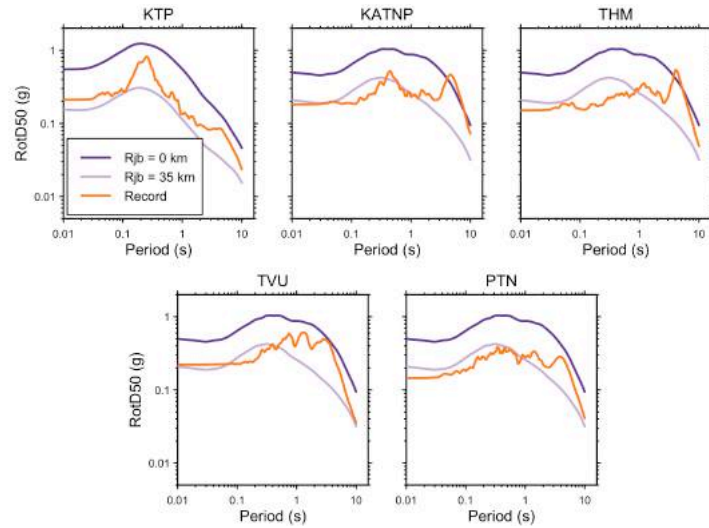


Fig. 10 – Comparison of the BSSA14 GMPE assuming both  $R_{jb} = 0$  km and  $R_{jb} = 35$  km to the recorded ground motions at the five strong motion stations in the Kathmandu Valley. The high-frequency components of the mainshock are better modeled with  $R_{jb} = 35$  km, while the long period components (3 sec or longer) are captured by the original BSSA14 using  $R_{jb} = 0$  km.

## 7. Acknowledgements

We thank Kishor Jaiswal for sharing the photo in Fig 1a. The accelerometer record at station KATPN was provided by the U.S. Geological Survey (USGS). The strong motion data at stations KTP, PTN, TVU and THM were processed by Michiko Shigefuji and Subeg Bijukchhen; the mainshock acceleration time series can be downloaded from <http://eprints.lib.hokudai.ac.jp/dspace/handle/2115/60622?locale=en&lang=en>; the aftershock time-series should be made available soon through the same portal. We acknowledge partial support of this work from the USGS/Caltech Cooperative Agreement (Sponsor Award Number G14AC00109), and from the GEER Association. Any use of trade, firm, or product names is for descriptive purposes only and does not imply endorsement by the U.S. Government.

## 8. References

- [1] Collins BD, Jibson RW (2015): Assessment of existing and potential landslide hazards resulting from the April 25, 2015 Gorkha, Nepal earthquake sequence. U.S. Geological Survey, U.S. Geological Survey Open-File Report 2015–1142, 50 p., <http://dx.doi.org/10.3133/ofr20151142>.
- [2] Moss RE, Thompson EM, Kieffer DS, Tiwari B, Hashash YM, Acharya I, Adhikari BR, Asimaki D, Clahan KB, Collins BD (2015): Geotechnical effects of the 2015 magnitude 7.8 Gorkha, Nepal, earthquake and aftershocks. *Seismol. Res. Lett.*, **86**(6), 1514–1523.

- [3] Hayes GP, Briggs RW, Barnhart WD, Yeck WL, McNamara DE, Wald DJ, Nealy JL, Benz HM, Gold RD, Jaiswal KS (2015): Rapid characterization of the 2015 Mw 7.8 Gorkha, nepal, earthquake sequence and its seismotectonic context. *Seismol. Res. Lett.*, **86**(6), 1557–1567.
- [4] McGowan SM, Jaiswal K, Wald DJ (2016): Macroseismic Intensity Assignments in Kathmandu Valley for the 2015 M7.8 Gorkha, Nepal Earthquake Based on Structural Damage Statistics. *Seismol. Res. Lett.*, **87**(2B), 512.
- [5] Szeliga W, Hough S, Martin S, Bilham R (2010): Intensity, magnitude, location, and attenuation in India for felt earthquakes since 1762. *Bull. Seismol. Soc. Am.*, **100**(2), 570–584.
- [6] Pandey MR, Molnar P (1988): The distribution of intensity of the Bihar-Nepal earthquake of 15 January 1934 and bounds on the extent of the rupture zone. *J. Nepal Geol. Soc.*, **5**(1), 22–44.
- [7] Chen W-P, Molnar P (1977): Seismic moments of major earthquakes and the average rate of slip in central Asia. *J. Geophys. Res.*, **82**(20), 2945–2969.
- [8] Chitrakar GR, Pandey MR (1986): Historical earthquakes of Nepal. *Bull Geol Soc Nepal*, **4**, 7–8.
- [9] Bilham R, Gaur VK, Molnar P (2001): Himalayan seismic hazard. *Science*, **293**(5534), 1442–1444.
- [10] Sapkota SN, Bollinger L, Klinger Y, Tapponnier P, Gaudemer Y, Tiwari D (2013): Primary surface ruptures of the great Himalayan earthquakes in 1934 and 1255. *Nat. Geosci.*, **6**(1), 71–76.
- [11] Bollinger L, Sapkota SN, Tapponnier P, Klinger Y, Rizza M, Van Der Woerd J, Tiwari DR, Pandey R, Bitri A, Bes de Berc S (2014): Estimating the return times of great Himalayan earthquakes in eastern Nepal: Evidence from the Patu and Bardibas strands of the Main Frontal Thrust. *J. Geophys. Res. Solid Earth*, **119**(9), 7123–7163.
- [12] Dixit A, Dwelly-Samant L, Nakarmi M, Pradhanang S, Tucker B (1998): The Kathmandu Valley Earthquake management plan. *Natl. Soc. Earthq. Technol. Nepal 37 Ppwww Prev. Netenglishprofessionalpublicationsv Php*.
- [13] Rana BJB (1935): Nepal Ko Maha Bhukampa (Great Earthquake of Nepal). *Kathmandu Nepal Nepali*.
- [14] Paudyal YR, Yatabe R, Bhandary NP, Dahal RK (2012): A study of local amplification effect of soil layers on ground motion in the Kathmandu Valley using microtremor analysis. *Earthq. Eng. Eng. Vib.*, **11**(2), 257–268.
- [15] Rajaure S, Asiamki D, Thompson EM, Hough S, Martin S, Ampuero JP, Dhital MR, Inbal A, Takai N, Shigefuji M, Bijukchhen S, Ichiyanaagi M, Sasatani T, Paudel L (2016): Characterizing the Kathmandu Valley sediment response through strong motion recordings of the 2015 Gorkha Earthquake sequence. *Tectonophysics*, doi: 10.1016/j.tecto.2016.09.030.
- [16] Pandey MR (2000): Ground response of Kathmandu Valley on the basis of microtremors. In *12th world conference on earthquake engineering (12 WCEE)*.
- [17] Paudyal YR, Bhandary NP, Yatabe R (2012): Seismic microzonation of densely populated area of Kathmandu Valley of Nepal using microtremor observations. *J. Earthq. Eng.*, **16**(8), 1208–1229.
- [18] Hagen T (1952): Preliminary note on the geological structure of Central Nepal.
- [19] Yoshida M, Igarashi Y (1984): Neogene to Quaternary lacustrine sediments in the Kathmandu Valley, Nepal. *J. Nepal Geol. Soc.*, **4**(Special issue), 73–100.
- [20] Moribayashi S, Maruo Y (1980): Basement topography of the Kathmandu Valley, Nepal-An application of gravitational method to the survey of a tectonic basin in the Himalayas. *J. Jpn. Soc. Eng. Geol.*, **21**(2), 80–87.
- [21] Hashash YM, Tiwari B, Moss RE, Asimaki D, Clahan KB, Kieffer DS, Dreger DS, Macdonald A, Madugo CM, Mason HB, Pehlivan M, Rayamajhi D, Acharya I, Adhikari B (2015): Geotechnical field reconnaissance: Gorkha (Nepal) earthquake of April 25, 2015 and related shaking sequence. *Geotech. Extreme Event Reconnaissance GEER Assoc. Rep. No GEER-040*, 1–250.
- [22] Sakai T, Gajurel AP, Tabata H, Upreti BN (2001): Small-amplitude lake-level fluctuations recorded in aggrading deltaic deposits of the Upper Pleistocene Thimi and Gokarna formations, Kathmandu Valley, Nepal. *J Nepal Geol Soc*, **25**(special issue), 43–52.
- [23] Nakata T, Kumura K, Rockwell T (1998): First successful paleoseismic trench study on active faults in the Himalaya. *Eos Trans AGU*, **79**, 45.

- [24] Takai N, Sawada K, Shigefuji M, Bijukchhen SM, Ichiyanagi M, Sasatani T, Dhakal YP, Rajaure S, Dhital MR (2015): Shallow underground structure of strong ground motion observation sites in the Kathmandu Valley. *NEPAL Geol. Soc.*, 50.
- [25] Dixit AM, Ringler AT, Sumy DF, Cochran ES, Hough SE, Martin SS, Gibbons S, Luetgert JH, Galetzka J, Shrestha SN (2015): Strong-motion observations of the M 7.8 Gorkha, Nepal, earthquake sequence and development of the N-SHAKE strong-motion network. *Seismol. Res. Lett.*, **86**(6), 1533–1539.
- [26] Bhattarai M, Adhikari LB, Gautam UP, Laurendeau A, Labonne C, Hoste-Colomer R, Sèbe O, Hernandez B (2015): Overview of the large 25 April 2015 Gorkha, Nepal, earthquake from accelerometric perspectives. *Seismol. Res. Lett.*, **86**(6), 1540–1548.
- [27] Avouac J-P, Meng L, Wei S, Wang T, Ampuero J-P (2015): Lower edge of locked Main Himalayan Thrust unzipped by the 2015 Gorkha earthquake. *Nat. Geosci.*, **8**(9), 708–711.
- [28] Sheehan AF, Torre T, Monsalve G, Schulte-Pelkum V, Bilham R, Blume F, Bendick R, Wu F, Pandey MR, Sapkota S (2008): Earthquakes and crustal structure of the Himalaya from the Himalayan Nepal Tibet seismic experiment (HIMNT). *J. Nepal Geol. Soc.*, **38**, 1–8.
- [29] De la Torre TL, Monsalve G, Sheehan AF, Sapkota S, Wu F (2007): Earthquake processes of the Himalayan collision zone in eastern Nepal and the southern Tibetan Plateau. *Geophys. J. Int.*, **171**(2), 718–738.
- [30] Rajaure S, Sapkota SN, Adhikari LB, Koirala B, Bhattarai M, Tiwari DR, Gautam U, Shrestha P, Maske S, Avouac JP (2013): Double difference relocation of local earthquakes in the Nepal Himalaya. *J Nepal Geol Soc*, **46**, 133–142.
- [31] Stöcklin J (1980): Geology of Nepal and its regional frame Thirty-third William Smith Lecture. *J. Geol. Soc.*, **137**(1), 1–34.
- [32] Mugnier J-L, Huyghe P, Gajurel AP, Upreti BN, Jouanne F (2011): Seismites in the Kathmandu basin and seismic hazard in central Himalaya. *Tectonophysics*, **509**(1), 33–49.
- [33] Boore DM (2010): Orientation-Independent, Nongeometric-Mean Measures of Seismic Intensity from Two Horizontal Components of Motion. *Bull. Seismol. Soc. Am.*, **100**(4), 1830–1835.
- [34] JICA M (2002): The study on Earthquake Disaster Mitigation in the Kathmandu Valley. *Kingd. Nepal Jpn. Int. Coop. Agency Minist. Home Aff. Nepal*.
- [35] Atkinson GM, Boore DM (2003): Empirical ground-motion relations for subduction-zone earthquakes and their application to Cascadia and other regions. *Bull. Seismol. Soc. Am.*, **93**(4), 1703–1729.
- [36] Zhao JX, Zhang J, Asano A, Ohno Y, Oouchi T, Takahashi T, Ogawa H, Irikura K, Thio HK, Somerville PG, Fukushima Y, Fukushima Y (2006): Attenuation Relations of Strong Ground Motion in Japan Using Site Classification Based on Predominant Period. *Bull. Seismol. Soc. Am.*, **96**(3), 898–913.
- [37] Atkinson GM, Macias M (2009): Predicted ground motions for great interface earthquakes in the Cascadia subduction zone. *Bull. Seismol. Soc. Am.*, **99**(3), 1552–1578.
- [38] Ghofrani H, Atkinson GM (2014): Ground-motion prediction equations for interface earthquakes of M7 to M9 based on empirical data from Japan. *Bull. Earthq. Eng.*, **12**(2), 549–571.
- [39] Abrahamson N, Gregor N, Addo K (2016): BC Hydro Ground Motion Prediction Equations for Subduction Earthquakes. *Earthq. Spectra*, **32**(1), 23–44.
- [40] Sharma ML, Douglas J, Bungum H, Kotadia J (2009): Ground-motion prediction equations based on data from the Himalayan and Zagros regions. *J. Earthq. Eng.*, **13**(8), 1191–1210.
- [41] Boore DM, Stewart JP, Seyhan E, Atkinson GM (2014): NGA-West2 equations for predicting PGA, PGV, and 5% damped PSA for shallow crustal earthquakes. *Earthq. Spectra*, **30**(3), 1057–1085.
- [42] Petersen MD, Moschetti MP, Powers PM, Mueller CS, Haller KM, Frankel AD, Zeng Y, Rezaeian S, Harmsen SC, Boyd O, Field N, Chen R, Rukstales K, Luco N, Wheeler RL, Williams RA, Olsen AH (2014): Documentation for the 2014 Update of the United States National Seismic Hazard Maps. U.S. Geological Survey Open-File Report 2014–1091, 243 p., <http://dx.doi.org/10.3133/ofr20141091>.